# Triboelectric Sensor for Self-Powered Tracking of Object Motion inside Tubing

**Yuanjie Su,[†,‡,⊥] Guang Zhu,[†,⊥] Weiqing Yang,[†,‡,⊥] Jin Yang,[†] Jun Chen,[†] Qingshen Jing,[†] Zhiming Wu,[‡] Yadong Jiang,[‡] and Zhong Lin Wang[†,§,*]**

[†]School of Materials Science and Engineering, Georgia Institute of Technology, Atlanta, Georgia 30332-0245, United States, [‡]State Key Laboratory of Electronic Thin Films and Integrated Devices, School of Optoelectronic Information, University of Electronic Science and Technology of China (UESTC), Chengdu 610054, China, and [§]Beijing Institute of Nanoenergy and Nanosystems, Chinese Academy of Sciences, Beijing, China. [⊥]Y. Su, G. Zhu, and W. Yang contributed equally to this work.

**ABSTRACT** We report a self-powered, single-electrode-based triboelectric sensor (SE-TES) array for detecting object motion inside of a plastic tube. This innovative, cost-effective, simple-designed SE-TES consists of thin-film-based ring-shaped Cu electrodes and a polytetrafluoroethylene (PTFE) tube. On the basis of the coupling effect between triboelectrification and electrostatic induction, the sensor generates electric output signals in response to mechanical motion of an object (such as a ball) passing through the electrodes. An array of Cu electrodes linearly aligned along the tube enables the detection of location and speed of the moving steel ball inside. The signal-to-noise ratio of this fabricated device reached $5.3 \times 10^3$. Furthermore, we demonstrated real-time monitoring and mapping of the motion characteristics of the steel ball inside the tube by using a seven-unit array of electrode channels arranged along the tube. Triggered by the output current signal, LED bulbs were utilized as real-time indicators of the position of a rolling ball. In addition, the SE-TES also shows the capability of detecting blockage in a water pipe. This work demonstrates potentially widespread applications of the triboelectric sensor in a self-powered tracking system, blockage detection, flow control, and logistics monitoring.

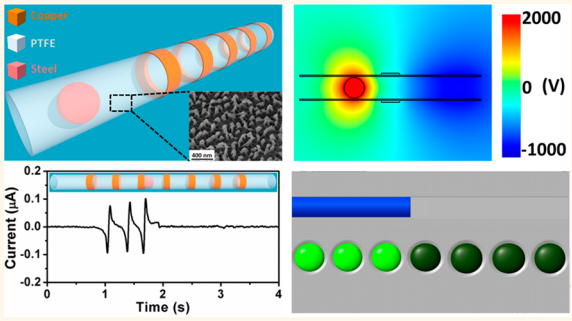


**KEYWORDS:** triboelectric effect · self-powered · tracking sensor · pipeline blockage detection

Developing a tracking and locating system is important for applications in transportation, logistics control, and flow monitoring.[1−4] Determining the location of an object by electronic means rather than direct video imaging is a fundamental demand in mobile computing and the Internet of Things.[5−8] The importance and promise of location-aware applications have led to the design and implementation of systems for optimizing detection modes, especially computational capabilities and sensing range.[9] Over the years, major research efforts have been based on detection mechanisms including optical, thermal, and magnetic.[10−12] Nevertheless, a common limitation is that most of these sensors require an external power source,[13,14] which poses challenges to longevity and mobility of the sensor. Recently, a class of self-powered sensors based on triboelectric nanogenerators (TENGs) was introduced.[15−22] By harvesting the mechanical energy from its working environment, the TENG-based sensors are able to work independently without an external power source. On the basis of a coupling effect between triboelectrification and electrostatic induction, they have been utilized for detecting catechin, mercury ions, change of a magnetic field, and spatial displacement.[23−27] However, few works have been done using the TENG for a self-powered real-time tracking system.

In this paper, we present a self-powered, single-electrode-based triboelectric sensor (SE-TES) that is based on rolling electrification and electrostatic induction. When a triboelectrically charged steel ball rolls along a polytetrafluoroethylene (PTFE) tube wrapped with ring-shaped Cu electrodes, it induces alternating flows of electrons between the Cu electrodes and the ground. The single-electrode-based structure requires no electric contact with the sensed

* Address correspondence to zlwang@gatech.edu.

Received for review February 4, 2014 and accepted March 4, 2014.

**Published online March 06, 2014**
**10.1021/nn500695q**

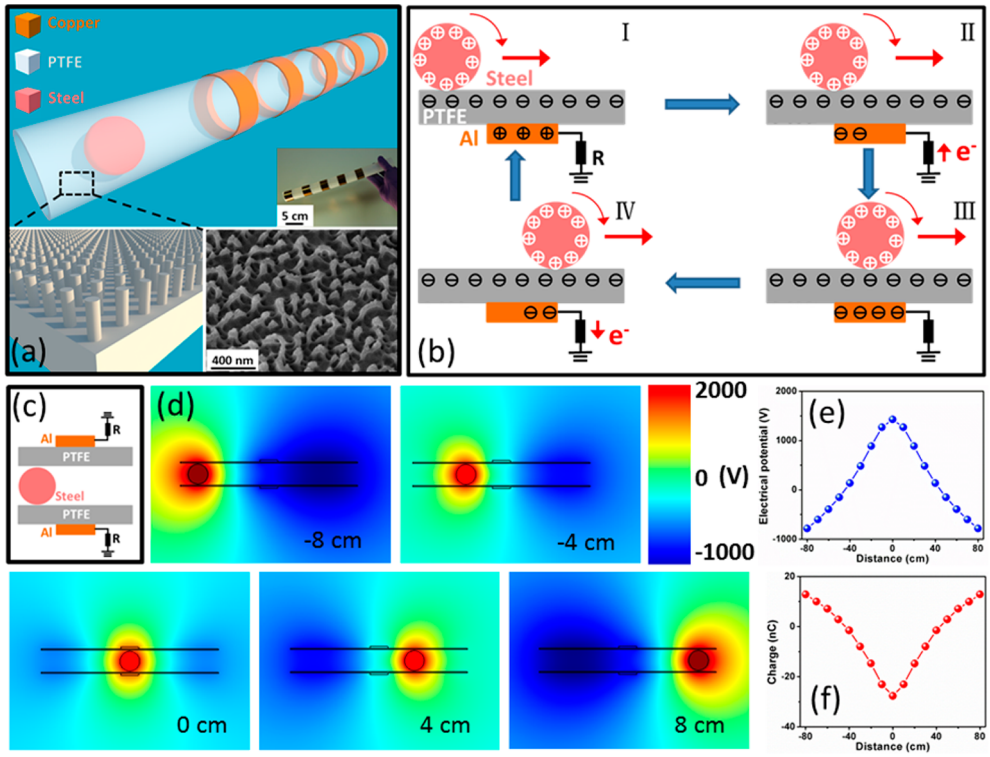


**Figure 1. Single-electrode-based triboelectric sensor (SE-TES). (a) Schematic diagram of the fabricated SE-TES. Inset: Photo of the real device, sketch, and SEM image of the PTFE surface with etched nanowire structure at a tilted view of 30°. (b) Working mechanism of SE-TES. (c) Schematic of the model for simulation. (d) Finite-element simulation of the potential distribution in the SE-TES under different positions of the steel ball inside the tube. (e) Calculated electrical potential on the Cu electrode as a function of the position of the steel ball. (f) Calculated charge quantity on the Cu electrode as a function of the position of the steel ball.**

object and allows outer Cu electrodes to cover any part of the PTFE tube, which considerably simplifies the structure and fabrication process. The working principle of the SE-TES was systematically investigated by experimental results and finite-element simulations. When the steel ball rolls across a Cu electrode, peak values of the open-circuit voltage and short-circuit current measured between the electrode and the ground reach 60 V and 0.4 $\mu$A, respectively. The moving speed of the steel ball can be obtained by an array of linear Cu electrodes along the PTFE tube. Furthermore, we demonstrated an application of the SE-TES by using seven electrode channels as a self-powered tracking system in real-time monitoring and mapping of the location of a rolling ball. The motion characteristics of the object, such as location and speed, can be obtained by analysis on the time-dependent electronic data. In addition, LED bulbs were utilized as direct tracking indicators for immediately showing the position of the object. Moreover, the SE-TES was able to identify the position of blockage in a tube filled with water. Therefore, this work explicitly presents the practicability of the SE-TES for potential applications in tracking systems, blockage detection, transportation monitoring, and health care.

## RESULTS AND DISCUSSION

A fabricated SE-TES is composed of a PTFE tube and Cu electrodes, as displayed in Figure 1a. The thin-film-based Cu electrodes are wrapped around the PTFE tube to form a linear array, as shown in the inset of Figure 1a. Here, PTFE and steel were selected as the contact materials for generating triboelectric charges due to their large difference in electron affinity.[28] As the triboelectrically charged steel ball rolls along the PTFE tube, electrons are induced to flow between the electrodes and the ground, resulting in a measurable alternating current. According to the scanning electron microscopy (SEM) image in Figure 1a, polymer nanowires are uniformly distributed on the inner surface of the PTFE tube, which have an average length of 310 nm and diameters ranging from 80 to 140 nm. The dry-etched nanowires on the PTFE surface increase the effective contacting area with the steel ball, enhancing the triboelectric charge density in the friction process. Figure 1b illustrates the working principle of the SE-TES. At the original position depicted in Figure 1b-I, due to the large difference in triboelectric polarity, PTFE attracts electrons from the steel ball, leaving net negative charges on the PTFE surface and an equal amount of positive charges on the steel ball. The generated negative triboelectric charges distribute

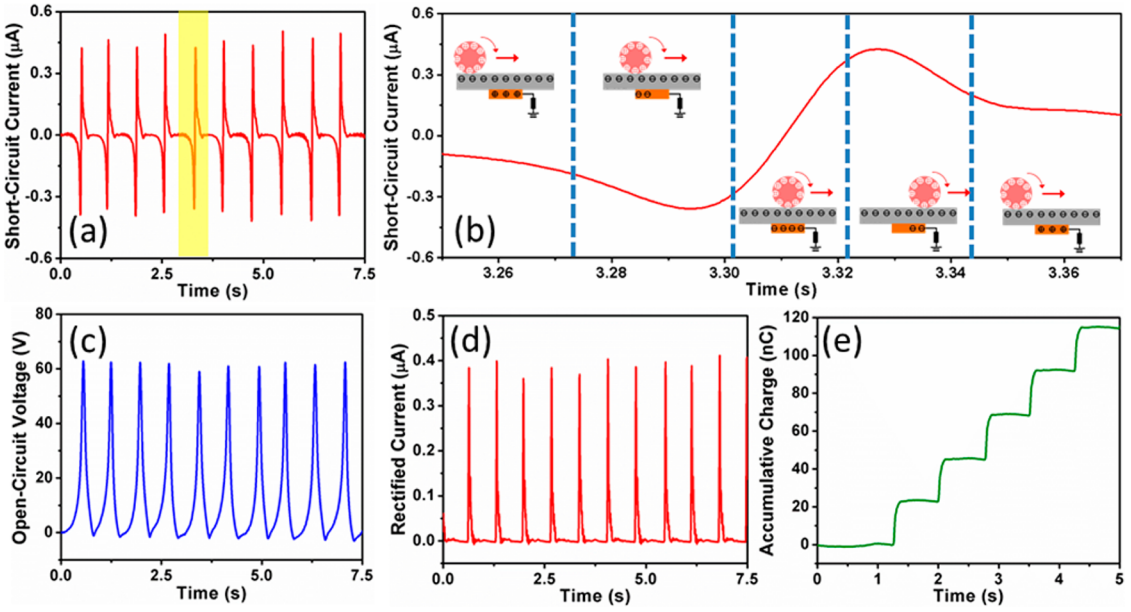


**Figure 2. Electrical measurement results of SE-TES with one electrode. (a) Short-circuit current and (b) enlarged view of a cycle highlighted in (a). (c) Open-circuit voltage. (d) Rectified current by a full-wave diode bridge. (e) Accumulative induced charges on S-TES enabled by a diode bridge. Note: The Cu electrodes were connected with positive probe of an electrometer, leaving the negative probe grounded.**

evenly on the PTFE tube and remain for an extended period of time owing to the insulating property of the polymer material.[28] These negative triboelectric charges on the PTFE tube induce positive charges on the Cu electrode from the ground as induced charges. Once the steel ball approaches the Cu electrode, the positive triboelectric charges on the steel ball will drive electrons to flow from the ground to the Cu electrode, for screening the electric field from the charged ball, as shown in Figure 1b-II.When the ball is aligned with the electrode, the negative charges reach the maximum quantity on the Cu electrode, as sketched in Figure 1b-III. As the steel ball starts to move away from the Cu electrode, the induced electrons will flow back to the ground, leaving fewer negative charges on the Cu electrode, as shown in Figure 1b-IV. Finally the device will return to its original state in Figure 1b-I as the ball is far from the electrode. Consequently, as the ball passes through, an alternating flow of electrons occurs between the electrode and the ground, which is the electric signal for indicating the approaching and leaving of the ball to/from the electrode.

To attain a more quantitative understanding of the proposed signal-generating process of the SE-TES, the electric potential distribution and charge transfer process for the device are investigated through numerical calculation using COMSOL. Figure 1c illustrates the proposed model for simulation. Figure 1d exhibits the simulation results of the electric potential distribution in the SE-TES when the ball is at five different distances away from the electrode. When the electrodes are fully aligned, the electric potential on the PTFE tube reaches a maximum. The electric potential is found to decrease dramatically as the distance between the steel ball and the electrode gets larger (Supporting Information, Figure S1). The calculated electric potential as a function of the distance is plotted in Figure 1e, in which the electric potential increases and then decreases with a peak value at the aligned position. Figure 1f shows the calculated charge quantity on the Cu electrode at different distances, which is in accordance with the aforementioned working process in Figure 1b.

To characterize the performance of the SE-TES in sensing moving objects, the electric output from one electrode as the steal ball rolls back and forth was systematically measured. Shown in Figure 2a, the short-circuit current exhibits peaks in alternating directions. An enlarged view in Figure 2b displays an entire cycle of the current and corresponding positions of the moving ball. Moving toward the Cu electrode produces a negative current peak, while departing causes a positive one, as illustrated by insets in Figure 2b. The interval between negative peak and positive peak corresponds to a status where the ball is rolling at the electrode-covered part of the tube, which brings about measurement error in location. The discrepancy between the diameter of the steel balls and the width of electrodes directly affects the interval and thus contributes to the accuracy of the position measurement. In order to obtain a fine accuracy, consistence between electrode width and ball diameter is highly demanded. The open-circuit voltage, as shown in Figure 2c, switches between zero and the maximum value of 60 V as the ball repeatedly passes through the electrode. The experimental results are fully consistent

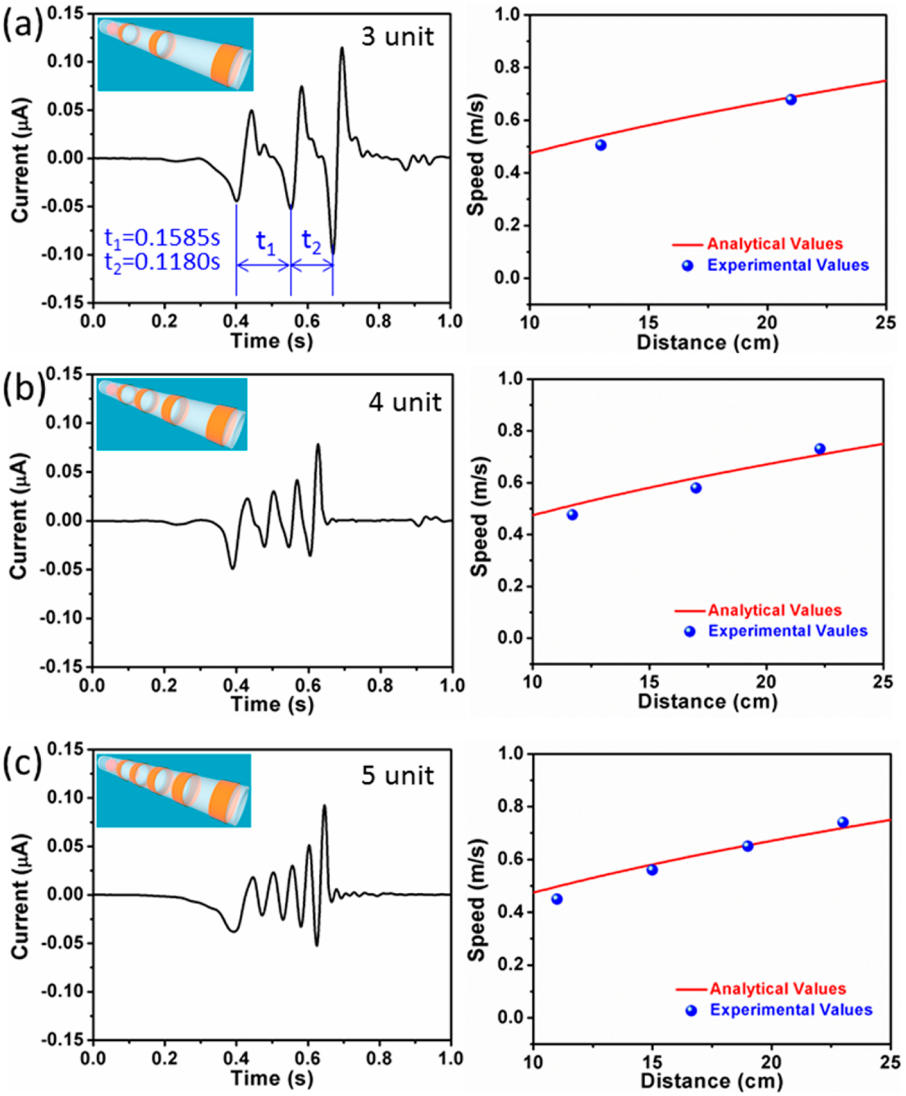


**Figure 3. Electrical measurement results of SE-TES with multiple grating electrodes. (a) Output current and corresponding measured speed of SE-TES with three grating electrodes. Inset: Schematic of the SE-TES structure. (b) Output current and corresponding measured speed of SE-TES with four grating electrodes. Inset: Schematic of the SE-TES structure. (c) Output current and corresponding measured speed of SE-TES with five grating electrodes. Inset: Schematic of the SE-TES structure.**

with the above theoretical analysis and numerical simulations. Enabled by a full-wave diode bridge, the ac electric output can be rectified to a pulsed direct current, as displayed in Figure 2d. With the diode bridge, the total accumulative induced charges, independent of moving direction, can be added up. According to Figure 2e, every step represents passing of the ball one time, generating average induced charges of 23.5 nC. To investigate the dependence of the electric output on the size of steel balls, the output performance of steel balls with diverse diameters was measured for the tracking sensor. As displayed in Figure S2, at a constant moving velocity of steel balls, the electric output shows a linear relationship with the diameter of steel balls. The amount of transferred charges ($\Delta Q$) is proportional to the diameter of the steel ball. On the basis of this linear relationship, the electric output for other size steel balls can be assumed preliminarily, leading to the prediction of detection limit.

If an array of Cu electrodes is applied along the PTFE tube with a certain interval in between, they can provide statistical information about the motion characteristics of a moving object. Cu electrodes with width of 2 cm for each are evenly distributed along the PTFE tube with a uniform interval and are connected in parallel to a positive probe of an electrometer. With the PTFE tube having a tilt angle of 15° to the horizontal plane (Supporting Information, Figure S3), the measured currents from devices having different numbers of electrodes are shown in Figure 3a–c, which correspond to reducing intervals of 8, 4.7, and 3 cm, respectively. The total counts of ac peaks are in accordance with the number of electrodes on the PTFE tube (Supporting Information, Figure S4). Analysis on Figure 3 provides twofold information. First, the

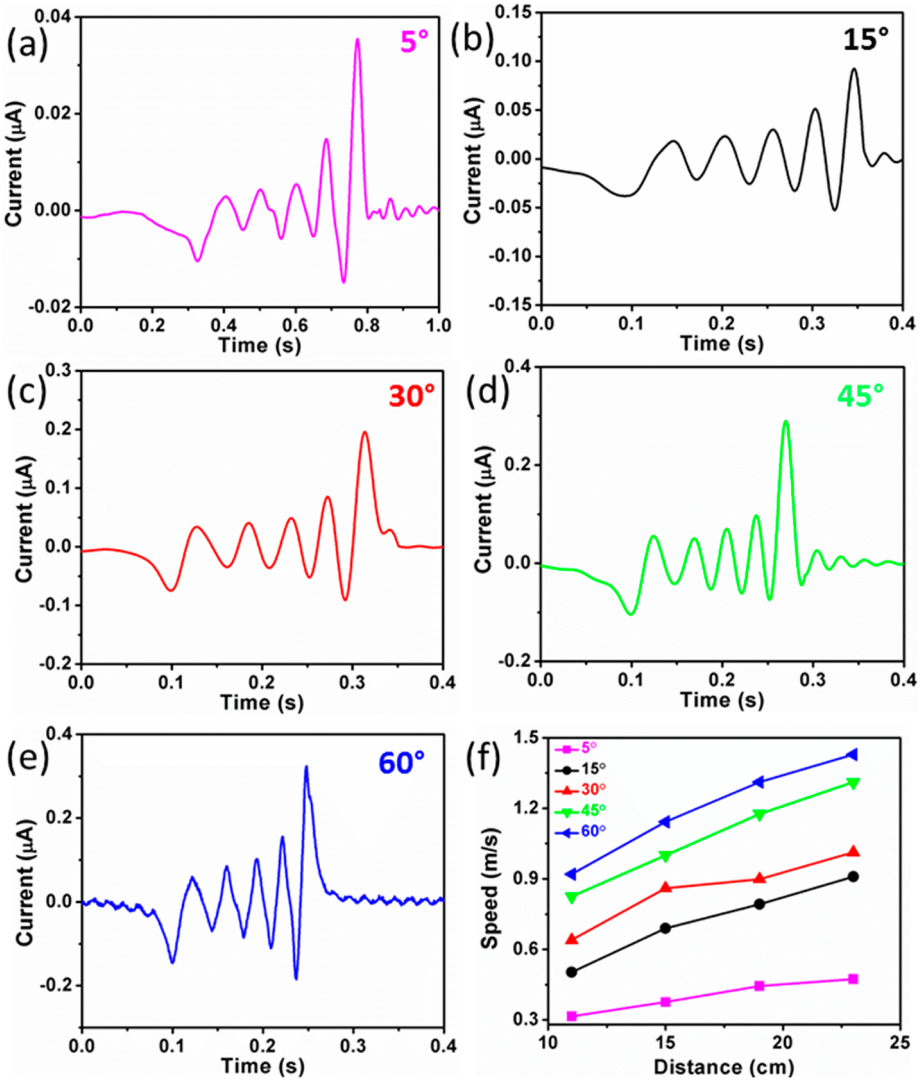


**Figure 4. Output current of SE-TES with five electrodes at tilt angles of (a) 5°, (b) 15°, (c) 30°, (d) 45°, and (e) 60°. (f) Plots of speed of a steel ball as a function of distance under different tilt angles.**

position of the ball can be identified because it has a one-to-one correspondence with the current signal, as discussed above. Second, by determining the time interval between two adjacent negative peaks, we can obtain the average moving velocity of the ball between two electrodes:

$$V_a = \frac{S}{t} \quad (1)$$

where $V_a$ is the average speed, $S$ is the spacing between the two electrodes, and $t$ is the time interval between two adjacent negative peaks. As the average speed is regarded as the instantaneous speed at the middle of the spacing, a plot of speed as a function of moving distance is expressed in Figure 3. Second, it is noteworthy that denser electrodes not only provide more positional information but also make the calculated average speed more closely approximated to the instantaneous speed. The amplitude of the output peaks gradually increases as the ball rolls through the tube. This is because the ball experiences an accelerated motion, which shortens the time of charge transfer and thus enhances the current.

To investigate the sensitivity and reliability of the SE-TES, we measured the current of the SE-TES at different tilting angles of the tube, as exhibited in Figure 4 (Supporting Information, Figure S5). With rising tilting angles, the steel ball rolls at higher accelerations, resulting in a monotonic growing trend of the current amplitude, as illustrated in Figure S4. As shown in Figure 4f, the measured average speed of the ball rises with an increasing slope when the tube is tilted at a higher angle, which reaches 0.91 and 1.43 m/s for the same traveling distance at different tilt angles of 15° and 60°, respectively.

To demonstrate potential applications of the SE-TES for a self-powered tracking system, we fabricated seven Cu electrodes along the PTFE tube of 150 cm in length for detecting and mapping the location of a moving object in real time (Figure 5a). The circuit

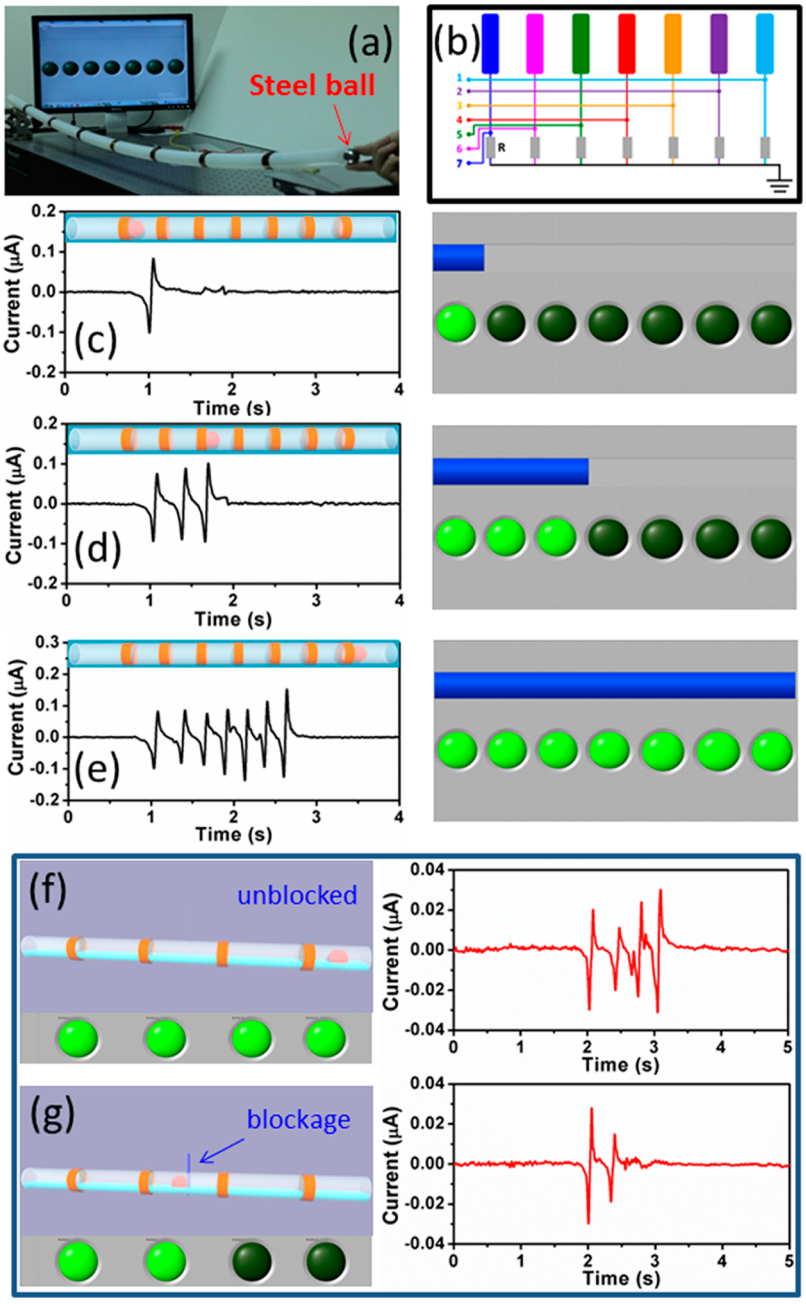


**Figure 5. Self-powered SE-TES-based tracking system. (a) Optical image of the fabricated SE-TES tracking system. (b) Circuit diagram of the tracking system. Measured output current and real-time location mapping when the steel ball arrives at the (c) first, (d) third, and (e) fifth electrode. (f) Detection of the steel ball rolling in an unblocked water pipe. (g) Detection of a steel ball rolling in a blocked water pipe, where the blockage is located between the second and third electrode.**

diagram of the system is shown in Figure 5b, in which an external load of 10 MΩ is connected between each electrode and the ground. The output currents from the seven channels were recorded and immediately displayed by indicators on a monitor. After being released at the higher end of the tube, the steel ball rolled inside the tube to its lower end and passed through the electrodes in sequence. When the steel ball arrived at the first electrode, a corresponding alternating current peak of 0.1 $\mu$A in amplitude was measured, as displayed in Figure 5c. The signal triggered the first locating light and progress bar, indicating that the ball had just passed the first electrode. Figure 5d and c show the current signals and the digital mapping results when the ball passes the third and the seventh electrodes, respectively (Supporting Information, Figure S6). Therefore, the positional information of the rolling ball can be immediately exhibited and directly perceived (see Supporting Information, Movie 1) without visual inspection of the ball. The tracking system can be further simplified by using LED bulbs as sensing indicators. With each

electrode individually connected to an LED bulb, the positional information of the ball can be directly visualized by LEDs that light up as the ball passes by (see Supporting Information, Movie 2).

To demonstrate the capability of the SE-TES of detecting object motion in a pipe partially filled with water, a PTFE tube having four electrodes was infused with tap water at a constant flow rate of 42 mL/s (Supporting Information, Figure S7). The water level was about 1.2 cm, which almost occupied one-third of the water pipe. The flow of tap water results in background noise in the electric measurement because of electrification between PTFE and the water molecules. The noise level is proportional to the flow rate, as shown in Figure S7. In addition, the influence of moisture ambient on the electric output of the SE-TES was also tested. As depicted in Figure S8, the output current decays slightly with increasing humidity. At a humidity ranging from 33% to 100% RH, the decrease of output current is less than 1 order of magnitude. This proves that the SE-TES is capable of working efficiently in a moist environment. When the steel ball rolled through an unblocked tube, as shown in Figure 5f, all positional indicators on the monitor were triggered, indicating that the pipe was clear, without blockage. However, if the tube was clogged in a location, the rolling ball was obstructed at the blockage site and triggered only some of the indicators (see Supporting Information, Movie 3). Such information can be used to quickly determine where a blockage occurs without thoroughly inspecting the entire the tube.

## CONCLUSIONS

In summary, we demonstrated a novel designed self-powered SE-TES based on rolling electrification between a PTFE tube and a steel ball. The rolling of steel ball along a PTFE tube leads to charge transfer between the Cu electrode and the ground, generating ac current peaks. By converting the mechanical motion into electrical output signal, the SE-TES delivers an open-circuit voltage of 60 V and a short-circuit current of 0.4 $\mu$A on each electrode. A linear array of Cu electrodes aligned along the tubing enables detection of location and speed of the steel ball inside. Increasing the number of electrodes gives more accurate and detailed information of object motion. On the basis of real-time recorded output current signals from the seven electrode channels, the position of the object can be displayed immediately as a mapping figure on the screen. By connecting them with electrodes, LEDs were utilized as real-time visible signs to indicate the passage of an object inside the tube. Furthermore, the SE-TES exhibits the capability of detecting blockage in a water pipe. This work pushes forward a significant step toward the application of triboelectric sensors in a self-powered tracking system, flow monitoring, and pipeline blockage detection.

## EXPERIMENTAL SECTION

**Nanowire-Based Surface Modification of PTFE Film.** Nanowires on the surface of PTFE were formed by using inductively coupled plasma (ICP) reactive ion etching. The PTFE film with a thickness of 50 $\mu$m was cleaned with isopropyl alcohol and deionized water, then blown dry with nitrogen gas. In the etching process, Au particles were deposited by using dc sputtering on the PTFE surface as a mask. Subsequently, a mixed gas including Ar, $O_2$, and $CF_4$ was introduced in the ICP chamber, with a corresponding flow rate of 15.0, 10.0, and 30.0 sccm, respectively. The PTFE film was etched for 15 s to obtain a nanowire structure on the surface. One power source of 400 W was used to yield a large density of plasma, while another 100 W was used to accelerate the plasma ions.

**Fabrication of a SE-TES.** The SE-TES consists of a PTFE tube and thin-film-based Cu electrodes. The tube and steel balls was purchased from McMaster. The inside and outside diameter of the tube is 2.54 and 2.78 cm, respectively. The diameter of the steel ball is 2.2 cm. The tube was cut along its axis into two parts and then the etched PTFE film was wrapped on the inner wall of the tube to form the PTFE tube. The Cu layer was deposited on the Kapton film as the Cu electrode by physical vapor deposition . The Cu coils were wound around the PTFE tube with a fixed interval to form grating electrodes.

**Characterization and Electrical Measurement of the SE-TES.** The morphology and nanostructure of the etched PTFE film were characterized by a Hitachi SU8010 field emission scanning electron microscope operated at 5 kV. The output performance of the TENG was measured using a Stanford Research Systems apparatus. SR560 and SR570 low-noise current amplifiers were used to record voltage and current, respectively.

**Simulation Model for the SE-TES.** The proposed model is based on a steel ball with a diameter of 2.2 cm and a 2 cm wide Cu electrode wrapped on a PTFE tube (inside diameter of 2.54 cm) with the same dimension (10 cm $\times$ 2.78 cm $\times$ 2.78 cm), as sketched in Figure 1c. The quantity of the triboelectric charges on the surfaces of the steel ball and PTFE tube is assumed to be $\pm$27.2 nC. The Cu electrode was connected to the ground.

*Conflict of Interest:* The authors declare no competing financial interest.

*Acknowledgment.* This work was supported by U.S. Department of Energy, Office of Basic Energy Sciences (DE-FG02-07ER46394), and the Thousands Talents program for pioneer researcher and his innovation team, China. Y. Su, Z. Wu, and Y. Jiang acknowledge the support of National Science Foundation of China *via* grant no. 61101029. Y. Su also would like to acknowledge the fellowship from the China Scholarship Council (CSC).

*Supporting Information Available:* Finite-element simulation of the potential distribution in SE-TES by COMSOL, electric output of the SE-TES with different electrodes under varied tilt angles, electric output of steel balls with diverse diameters, photographs of the device for detection of blockage in a water pipe, and output performance of SE-TES under a moist ambient. This information is available free of charge *via* the Internet at http://pubs.acs.org.

## REFERENCES AND NOTES

1. Betke, M.; Haritaoglu, E.; Davis, L. S. Real-Time Multiple Vehicle Detection and Tracking from a Moving Vehicle. *Mach. Vis. Appl.* **2000**, *12*, 69–83.

2. Hightower, J.; Borriello, G. Location Systems for Ubiquitous Computing. *Computer* **2001**, *34*, 57–66.
3. Mori, K.; Deguchi, D.; Akiyama, K.; Kitasaka, T.; Maurer, C. R.; Suenaga, Y.; Takabatake, H.; Mori, M.; Natori, H. Hybrid Brochoscope Tracking Using a Magnetic Tracking Sensor and Image Registration. *Lect. Notes Comput. Sci.* **2005**, *3750*, 543–550.
4. Jin, G. Y.; Lu, X. Y.; Park, M. S. Dynamic Clustering for Object Tracking in Wireless Sensor Networks. *Lect. Notes Comput. Sci.* **2005**, *4239*, 200–209.
5. Round, S.; Steingart, D.; Frechette, L.; Wright, P.; Rabaey, J. Power Source for Wireless Sensor Networks. *Lect. Notes Comput. Sci.* **2004**, *920*, 1–17.
6. Shen, G. P.; Qin, M.; Huang, Q.-A. A Cross Type Thermal Wind Sensor with Self-Testing Function. *IEEE Sens. J.* **2010**, *10*, 340–346.
7. Meng, B.; Tang, Wei.; Too, Z. H.; Zhang, X. S.; Han, M. D.; Liu, W.; Zhang, H. X. A Transparent Single-Friction-Surface Triboelectric Generator and Self-Powered Touch Sensor. *Energy Environ. Sci.* **2013**, *6*, 3235–3240.
8. Zhang, X. S.; Han, M. D.; Wang, R. X.; Zhu, F. Y.; Li, Z. H.; Wang, W.; Zhang, H. X. Frequency-Multiplication High-Output Triboelectric Nanogenerator for Sustainably Powering Biomedical Microsystems. *Nano Lett.* **2013**, *13*, 1168–1172.
9. Guo, Z.; Zhou, M. C.; Zakrevski, L. Optimal Tracking Interval for Predictive Tracking in Wireless Sensor Network. *IEEE Commun. Lett.* **2005**, *9*, 805–807.
10. Yaralioglu, G. G.; Atalar, A.; Manalis, S. R.; Quate, C. F. Analysis and Design of an Interdigital Cantilever as a Displacement Sensor. *J. Appl. Phys.* **1998**, *83*, 7405–7415.
11. Lantz, M. A.; Binnig, G. K.; Despont, M.; Drechsler, U. A Micromechanical Thermal Displacement Sensor with Nanometre Resolution. *Nanotechnology* **2005**, *16*, 1089–1094.
12. Miller, M. M.; Prinz, G. A.; Lubitz, P.; Hoines, L.; Krebs, J. J.; Cheng, S. F.; Parsons, F. G. Novel Absolute Linear Displacement Sensor Utilizing Giant Magnetoresistance Elements. *J. Appl. Phys.* **1997**, *81*, 4284–4286.
13. Wang, Z. L.; Wu, W. Nanotechnology-Enabled Energy Harvesting for Self-Powered Micro/Nanosystems. *Angew. Chem., Int. Ed.* **2012**, *51*, 11700–11721.
14. Yang, Y.; Zhou, Y.; Wu, J. M.; Wang, Z. L. Single Micro/Nanowire Pyroelectric Nanogenerator as Self-Powered Temperature Sensors. *ACS Nano* **2012**, *6*, 8456–8461.
15. Fan, F. R.; Tian, Z. Q.; Wang, Z. L. Flexible Triboelectric Generator. *Nano Energy* **2012**, *1*, 328–334.
16. Zhu, G.; Chen, J.; Liu, Y.; Bai, P.; Zhou, Y. S.; Jing, Q. S.; Pan, C. F.; Wang, Z. L. Linear-Grating Tiboelectric Generator Based on Sliding Electrification. *Nano Lett.* **2013**, *13*, 2282–2289.
17. Zhu, G.; Lin, Z. H.; Jing, Q. S.; Bai, P.; Pan, C. F.; Yang, Y.; Zhou, Y. S.; Wang, Z. L. Toward Large-Scale Energy Harvesting by a Nanoparticle-Enhanced Triboelectric Nanogenerator. *Nano Lett.* **2013**, *13*, 847–853.
18. Su, Y. J.; Yang, Y.; Zhong, X. D.; Zhang, H. L.; Wu, Z. M.; Jiang, Y. D.; Wang, Z. L. Fully Enclosed Cylindrical Single-Electrode-Based Triboelectric Nanogenerator. *ACS Appl. Mater. Interfaces* **2013**, *6*, 553–559.
19. Lin, L.; Xie, Y. N.; Wang, S. H.; Wu, W. Z.; Niu, S. M.; Wen, X. N.; Wang, Z. L. Triboelectric Active Sensor Array for Self-Powered Static and Dynamic Pressure Detection and Tactile Imaging. *ACS Nano* **2013**, *7*, 8266–8274.
20. Zhang, H. L.; Yang, Y.; Hou, T. C.; Su, Y. J.; Hu, C. G.; Wang, Z. L. Triboelectric Nanogenerator Built inside Clothes for Self-Powered Glucose Biosensors. *Nano Energy* **2013**, *2*, 1019–1024.
21. Zhang, H. L.; Yang, Y.; Su, Y. J.; Chen, J.; Hu, C. G.; Wu, Z. K.; Liu, Y.; Wong, C. P.; Wang, Z. L. Triboelectric Nanogenerator as Self-Powered Active Sensors for Detecting Liquid/Gaseous Water/Ethanol. *Nano Energy* **2013**, *2*, 693–701.
22. Meng, B.; Tang, W.; Zhang, X. S.; Han, M. D.; Liu, W.; Zhang, H. X. Self-Powered Flexible Printed Circuit Board with Integrated Triboelectric Generator. *Nano Energy* **2013**, *6*, 1101–1106.
23. Lin, Z. H.; Zhu, G.; Zhou, Y. S.; Yang, Y.; Bai, P.; Chen, J.; Wang, Z. L. A Self-Powered Triboelectric Nanosensor for Mercury Ion Detection. *Angew. Chem., Int. Ed.* **2013**, *125*, 5169–5173.
24. Lin, Z. H.; Xie, Y.; Yang, Y.; Wang, S.; Zhu, G.; Wang, Z. L. Enhanced Triboelectric Nanogenerator and Triboelectric Nanosensor Using Chemically Modified $TiO_2$ Nanomaterials. *ACS Nano* **2013**, *7*, 4554–4560.
25. Yang, Y.; Lin, L.; Zhang, Y.; Jing, Q.; Hou, T.-C.; Wang, Z. L. Self-Powered Magnetic Sensor Based on a Triboelectric Nanogenerator. *ACS Nano* **2012**, *6*, 10378–10383.
26. Su, Y. J.; Yang, Y.; Zhang, H. L.; Xie, Y. N; Wu, Z. M.; Jiang, Y. D.; Fukata, N.; Bando, Y.; Wang, Z. L. Enhanced Photodegradation of Methyl Orange with $TiO_2$ Nanoparticles using a Triboelectric Nanogenerator. *Nanotechnology* **2013**, *24*, 295401.
27. Yang, Y.; Zhang, H. L.; Chen, J.; Jing, Q. S.; Zhou, Y. S.; Wen, X. N.; Wang, Z. L. Single-Electrode-Based Sliding Triboelectric Nanogenerator for Self-Powered Displacement Vector Sensor System. *ACS Nano* **2013**, *7*, 7342–7351.
28. Saurenbach, F.; Wollmann, D.; Terris, B. D.; Diaz, A. F. Force Microscopy of Ion-Containing Polymer Surfaces: Morphology and Charge Structure. *Langmuir* **1992**, *8*, 1199–1203.